Neuron, Vol. 19, 293–306, August, 1997, Copyright ©1997 by Cell Press

Dynamic Processes Shape Spatiotemporal Properties of Retinal Waves

Marla B. Feller,*‡ Daniel A. Butts,† Holly L. Aaron,* Daniel S. Rokhsar,† and Carla J. Shatz*
*Howard Hughes Medical Institute
and Department of Molecular and Cell Biology
†Life Sciences Division
Lawrence Berkeley National Laboratory
and Department of Physics
University of California
Berkeley, California 94720

Summary

In the developing mammalian retina, spontaneous waves of action potentials are present in the ganglion cell layer weeks before vision. These waves are known to be generated by a synaptically connected network of amacrine cells and retinal ganglion cells, and exhibit complex spatiotemporal patterns, characterized by shifting domains of coactivation. Here, we present a novel dynamical model consisting of two coupled populations of cells that quantitatively reproduces the experimentally observed domain sizes, interwave intervals, and wavefront velocity profiles. Model and experiment together show that the highly correlated activity generated by retinal waves can be explained by a combination of random spontaneous activation of cells and the past history of local retinal activity.

Introduction

The final steps in the construction of adult neural circuitry frequently require neural activity (Goodman and Shatz, 1993; Katz and Shatz, 1996). Early in development, this activity can exist in the form of spontaneously generated signals. In particular, spontaneous, rhythmic bursts of action potentials have been recorded from developing retinal ganglion cells in a variety of vertebrate species (Masland, 1977; Maffei and Galli-Resta, 1990; Meister et al., 1991; Sernagor and Grzywacz, 1996). This spontaneous retinal activity is relayed to more central visual structures (Mooney et al., 1996), where it is thought to drive the activity-dependent synaptic remodeling that produces the adult patterns of connectivity (Cline, 1991; Mooney et al., 1993; Shatz, 1996).

This spontaneous activity in the developing retina can be monitored across large areas using a multi-electrode array (Meister et al., 1991; Wong et al., 1993) or fluorescence imaging of calcium indicators (Wong et al., 1995; Feller et al., 1996). Through the use of these techniques, it has been shown that long before the onset of photoreceptor function, spontaneous bursts of action potentials propagate across the ganglion cell layer in a wavelike manner that produces highly correlated firing among neighboring ganglion cells (Meister et al., 1991; Wong et al., 1995; Feller et al., 1996). The generation of this spontaneous activity requires activation of a horizontal synaptic circuit thought to involve at least two retinal cell types: amacrine cells and ganglion cells (Wong et al., 1995; Feller et al., 1996). At the earliest times when waves are present, there are no evident synapses from bipolar to amacrine or to ganglion cells, though there are likely to be functional synapses between amacrine cells or from amacrine to ganglion cells (Maslim and Stone, 1986; Nishimura and Rakic, 1987; Hutchins et al., 1995). Cholinergic amacrine cells (Dann, 1989; Mitrofanis et al., 1989; Feller et al., 1996), as well as neuronal nicotinic receptors (Hamassaki-Britto et al., 1994), are known to be present at these early ages. Cholinergic synaptic transmission is required for the initiation of activity; it is also required for wave propagation across the retina and is therefore involved in the horizontal coupling of cells (Feller et al., 1996).

Although there is strong evidence for a network of amacrine and retinal ganglion cells in producing retinal waves, exactly how the two cells cooperate to generate the complex spatiotemporal dynamics is unknown. For example, as seen by fluorescence imaging, retinal waves propagate over finite regions of tissue, which we call domains. Since the domain boundaries change gradually over time, discrete functional units of cells evidently cannot account for the spatial properties of the waves (Feller et al., 1996). Although a refractory period appears to be responsible for some domain boundaries (Feller et al., 1996), other waves stop in regions without apparent recent activity. What determines the boundaries that do not appear to be defined by earlier waves?

Here, we present a novel two-layer model of the developing retina that reproduces the spatiotemporal patterns of retinal waves and thereby demonstrates how the retinal circuitry can generate these patterns. We first show that the retina is a homogeneous substrate with respect to wave initiation, propagation, and termination. We then present a model of the developing retina as a spontaneously active network consisting of two coupled homogeneous populations of cells. A computer simulation of this model robustly reproduces the observed spatiotemporal behavior of the waves, as demonstrated by comparing the statistical properties of retinal waves and the simulated waves. Finally, we argue that a specific class of one-layer models cannot account for these observed properties.

Results

Initiation Locations and Wave Boundaries Are Randomly Distributed across the Retina

Retinal waves initiate from local areas of tissue and propagate over spatially restricted regions, which we have called domains (Feller et al., 1996). Waves induce an increase in $[Ca^{2+}]_i$ in individual ganglion cells on the order of 50 nM (Wong et al., 1995); this increase in $[Ca^{2+}]_i$ causes a substantial change in fura-2 fluorescence (ΔF), which allows us to monitor the spatial extent of wave

‡To whom correspondence should be addressed.

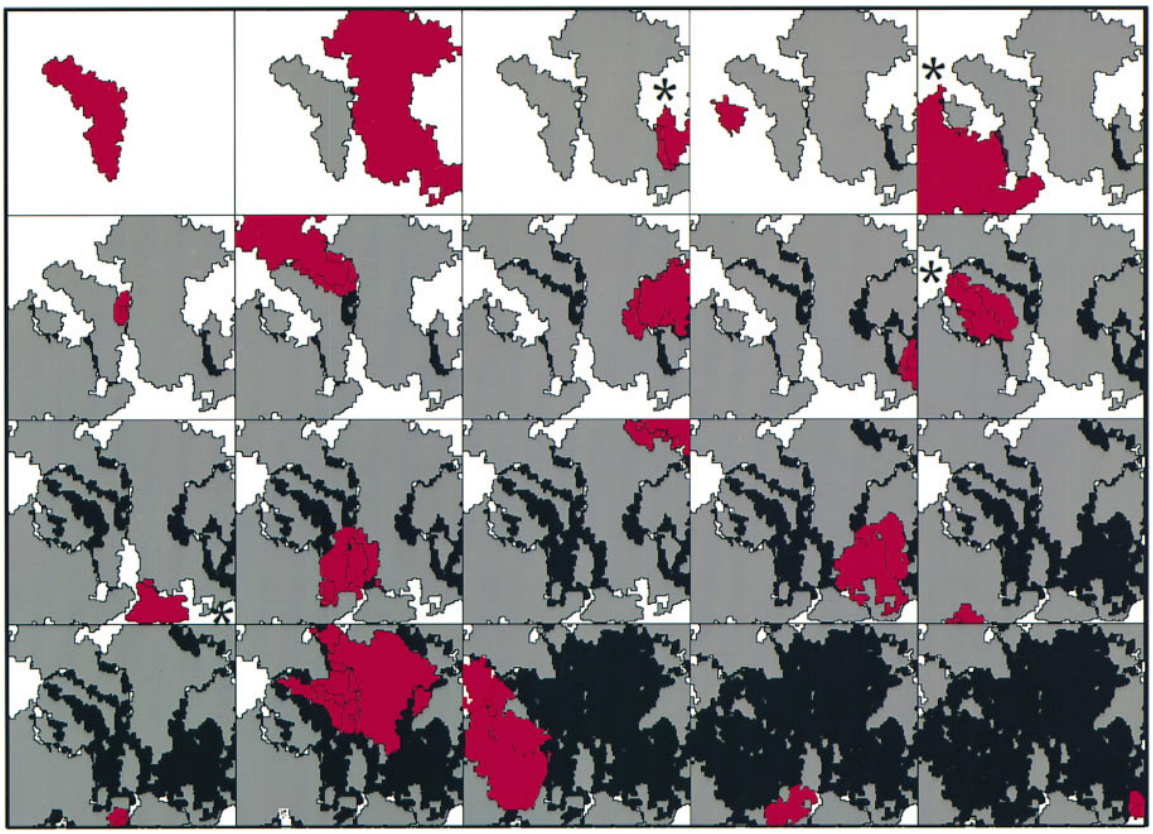

Figure 1. Definition of Domains

Spontaneous waves measured with fluorescence imaging in a P2 ferret retina loaded with fura-2AM. A mosaic of domains is created by sequential spontaneous waves. The red domain in each frame corresponds to a new wave arising in the same region of retina monitored with fura-2 imaging. Overlapping regions in which more than one wave occurs are shown in black. The entire sequence corresponds to 2 min of recording (read from left to right, top row first). The fact that almost the entire region is black after 2 min indicates that domain boundaries change constantly over time. Asterisks indicate regions where waves terminate despite lack of recent activity. The total field of view is 1.2 mm × 1.4 mm. The time evolution of the first two waves in this series can be viewed directly in Segment 1 of the video accompanying this paper at www.neuron.org.

propagation across several square millimeters of the retina. The changes in $[Ca^{2+}]_i$ monitored by fluorescence imaging are an indirect measure of membrane depolarizations, since these changes in fluorescence are simultaneous with barrages of synaptic currents onto ganglion cells (Feller et al., 1996). Since the waves induce a fairly uniform ΔF and stop abruptly, wave boundaries can be determined unambiguously (see Figure 1A; Feller et al., 1996). To examine the spatial configuration of domains, consider a sequence of waves that was imaged over a period of 2 min (Figure 1; movies of these waves can be viewed in Segment 1 of the video accompanying this paper at www.neuron.org). As previously described (Feller et al., 1996), each individual wave defines a domain (Figure 1, red areas); over time, the entire retinal ganglion cell layer is tiled by these domains (Figure 1, gray areas). Over periods of time of <1 min, there is very little overlap between new domains and the domains of earlier waves (black areas in Figure 1, top two rows). Over longer periods of time, new waves can encroach significantly into domains defined by earlier waves (Figure 1, bottom 2 rows). This implies that the retina has a refractory period which restricts wave propagation (Feller et al., 1996). We define the refractory period as the minimum time interval following the activation of an area of retina during which it cannot participate in a wave. Similar analysis of 11 retinas shows that this refractory period ranges from 40–60 s (data not shown; see also Feller et al., 1996). Waves in the ganglion cell layer can also occasionally terminate in regions without detectable recent activity (see Figure 1, asterisks); these boundaries do not appear to be set by the refractory period. The presence of shifting domain boundaries suggests that there are no fixed structures within the retina that limit wave propagation.

Figure 2 demonstrates this point more directly. All waves ($n = 11$) passing through a given area of mid- to peripheral retina were superimposed (Figure 2A). It is clear that the boundaries of these waves are all different, and the pattern of activity is both isotropic and spatially decaying, consistent with a homogeneous substrate. To show that this distribution of domains is independent of direction, we calculated the probability that a wave that includes the center point of Figure 2A also passes

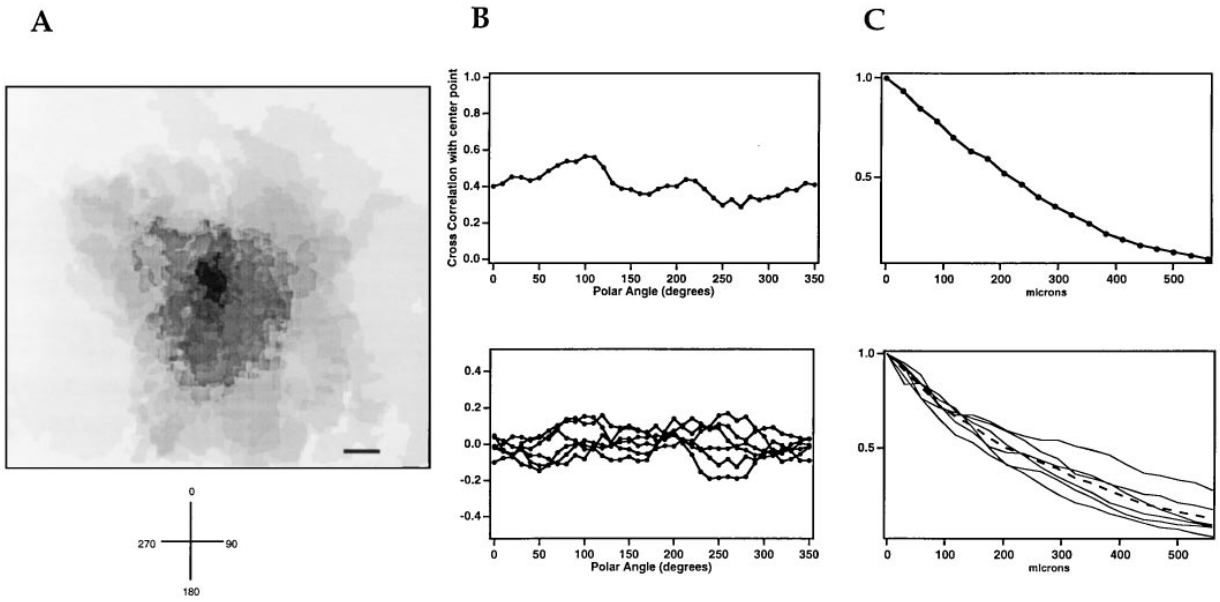

Figure 2. Spatial Distribution of Cells Correlated by Waves

(A) Superposition of all waves that passed through the center of an imaged area of retina during a 20 min recording session. The darkest regions correspond to the largest number of overlapping waves.

(B and C) Isotropy and range of wave propagation for the retina shown in (A).

(B, top) The correlation at each angle was computed by taking the product of the number of overlapping waves at the center with the number of overlapping waves at a given angle, averaged over distances up to 600 μm, and normalized to the square of the number of overlapping waves at the center.

(B, bottom) Results for five retinas.

(C, top) The correlation at each distance was computed by taking the product of the number of overlapping waves at the center with the number of overlapping waves at a given distance, averaged over all angles, and normalized to the square of the number of overlapping waves at the center.

(C, bottom) The results for 5 retinas, with the average radial correlation function shown by the dotted line. The 1/e of the average radial distribution occurs at 350 μm. Scale bar, 200 μm.

through a point at a given distance and angular position from this center. Figure 2B shows this correlation function averaged over all distances along a given direction. This analysis emphasizes that there is no preferred direction of propagation across this region. Similar measurements for several retinas (n = 5) confirm this conclusion (Figure 2B, bottom). To measure the range over which activity is spatially correlated, we also computed the correlation as a function of distance, averaged over all propagation directions (Figure 2C). The results averaged over five retinas are well fit by an exponential with a decay length of 350 μm (Figure 2C, bottom; dotted line). This length is a measure of the characteristic dimensions of a domain. Taken together, the results of Figure 2 show that the spontaneous activity in the retinal ganglion cell layer is statistically homogeneous and isotropic.

Waves initiate at randomly distributed locations across the retina. The spatial distribution of >100 consecutive initiation sites for one retina is shown in Figure 3A. An initiation site is defined as the centroid of the smallest resolvable area of initial change in fluorescence, whose size (0.026 ± 0.015 mm^2; n = 200 waves, 4 retinas) corresponds to ~70 cells in the ganglion cell layer. Over the entire recording period, only one wave initiated at each site; there is no evidence for the existence of special zones where waves would be repeatedly initiated. To test whether the initiation sites are randomly distributed, we constructed a histogram of all inter-initiation site distances. The results for one retina (Figure 3B), and for a total of 5 retinas (data not shown), are consistent with a uniform, random distribution of initiation sites (Figure 3B; solid line).

The above analysis suggests that the spatial properties of the waves are not determined by fixed structural units within the retina such as pacemakers or recurring domains. We therefore hypothesize that every location within the developing retina contains the circuitry capable of initiating and supporting waves, and that the global spatial patterns and dynamics of waves are determined by the local history of retinal activity.

A Two-Layer Model Reproduces the Spatiotemporal Properties of Retinal Waves

Can the observed complexity of retinal wave patterns—namely, the periodicity, domain size, compactness, and wavefront velocity—be reproduced by modeling a simple neuronal network based on the above hypothesis? Here, we introduce a two-layer readout model, comprised of two distinct populations of cells having properties that correspond to the ganglion and amacrine cells known to be involved in the neural circuit that generates waves (Wong et al., 1995; Feller et al., 1996). The two-layer readout model is based on many assumptions

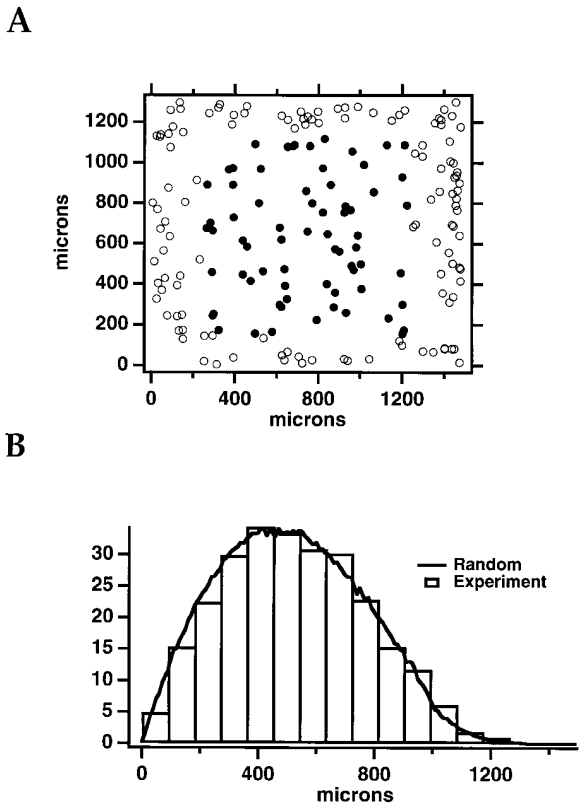

Figure 3. Distribution of Initiation Sites of Waves

(A) Open and closed circles correspond to the locations of the initiation sites of 50 waves over a 1.4 mm × 1.2 mm area of a P2 retina. (B) The distribution of distances calculated between all pairs of initiaton sites. Only waves initiated in the central 1 mm^2 were included (closed circles) to exclude waves that may have initiated outside and then propagated into the imaged area (open circles). The solid line corresponds to the distribution of distances computed for a random set of points in the same geometrical area. Bin size corresponds to 90 μm, the minimum detectable initation site radius.

about the physiological properties and connectivity of amacrine cells and ganglion cells in the immature retina. (For a model of wave generation based on biophysical properties of ganglion cells, see Burgi and Grzywacz, 1994.) Our assumptions and an assessment of their validity can be found in the Discussion.

Since our goal is to describe the system at time scales related to the waves (s) rather than the underlying cellular events (ms), the model is correspondingly coarse, and treats each cell within the network as a simple unit whose excitation level (analogous to depolarization away from resting membrane potential) is increased by excitatory inputs and decays exponentially with time. Horizontal coupling in the network is determined by connections between amacrine cells, and between amacrine and ganglion cells, as illustrated schematically in Figure 4A. As much as possible, the characteristic lengths and times of the model have been chosen to correspond to available anatomical and physiological data (see Experimental Procedures).

Both model cell types have a characteristic threshold. A model amacrine cell can reach its threshold in two ways: either through an intrinsic spontaneous depolarization or through the cumulative effect of excitatory inputs from other nearby amacrine cells. Afterwards, it enters a refractory period during which it cannot be depolarized. Only when an amacrine cell exceeds its threshold can it cause other nearby amacrine cells and ganglion cells to depolarize via synaptic coupling.

A model ganglion cell receives inputs only from amacrine cells and has neither a refractory period nor the ability to depolarize spontaneously. The ganglion cell layer serves as a passive filter of the amacrine cell layer activity (note, there is no coupling between ganglion cells), and we therefore refer to the ganglion cell layer as a readout layer. We also assume that a ganglion cell participates in a wave only when its excitation level exceeds a threshold. In our model, subthreshold amacrine and ganglion cell activity is not detectable. A more detailed discussion of the model is found in the Experimental Procedures.

The model and the experiment are qualitatively similar in that the properties of the simulated waves—their shape, frequency, rate of movement across the retina, etc.—are essentially indistinguishable from those observed experimentally. This similarity is best appreciated by viewing the movies of the simulated and experimentally recorded waves (see www.neuron.org).

Four sequential waves generated by the simulation are presented in Figure 4B. While our imaging experiments are limited to visualizing cells in the ganglion cell layer that undergo large changes in $[Ca^{2+}]_i$, we can derive a more complete analysis of the activity with the model, since otherwise hidden activity in the amacrine cell layer can be measured in simulations. The top row in Figure 4B contains superimposed activity maps from the amacrine and ganglion cell layers. Each frame displays those amacrine cells (red) that provided the excitatory input to the set of ganglion cells that reached threshold during the wave (blue). Also pictured are the amacrine cells whose depolarization to threshold was independent of the wave (gray dots). These cells spontaneously depolarized during the wave, but at too low a density to excite nearby ganglion cells above their threshold. The convergence and divergence of projections between the two layers (Figure 4A), together with the thresholding of the ganglion cell layer response, turn a sparse wave in the amacrine cell layer into a contiguous ganglion cell layer wave, reproducing the character of the experimentally observed waves.

The model predicts that wave initiation and propagation are strongly influenced by the past history of amacrine cell activity, both associated with and independent of waves. In the context of our model, this past history is represented by the density of nonrefractory amacrine cells in a region. The lower frames in Figure 4B show the fraction of nonrefractory amacrine cells that are present in the time step just preceding the wave shown in the top frame. Red regions have a high fraction ($\sim$50%) and blue regions a low fraction ($<$20%) of nonrefractory amacrine cells. Waves are more likely to initiate in red than blue regions, since they contain a larger pool of available amacrine cells that could spontaneously depolarize. In this sense, the red regions represent

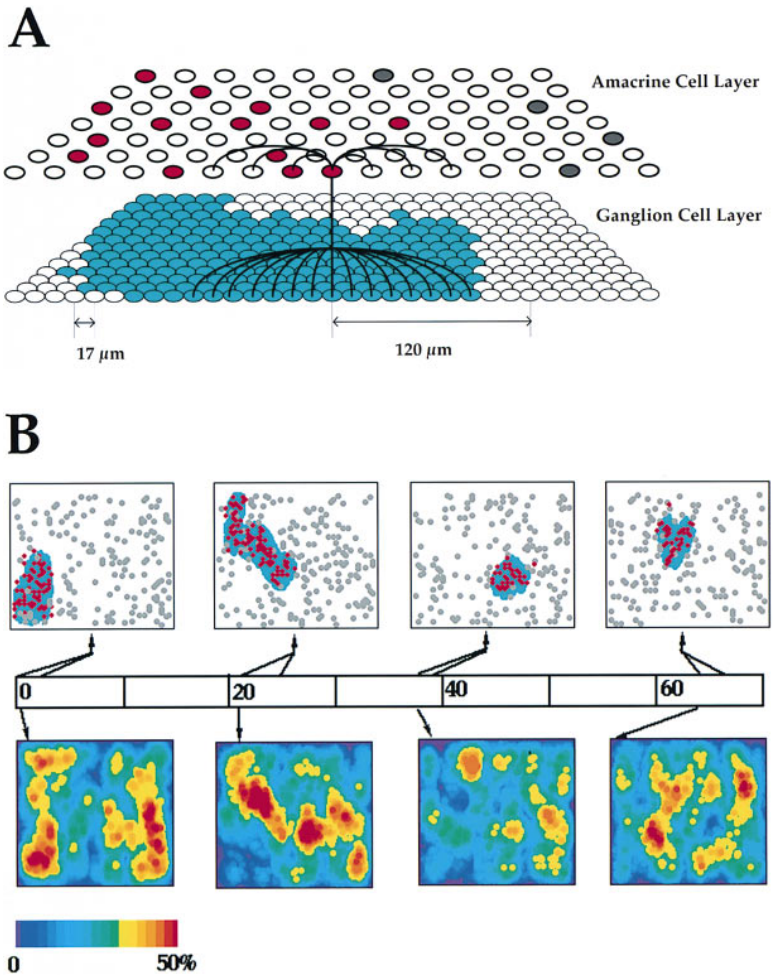

Figure 4. Model and Simulated Waves of Activity

(A) Model schematic. The model consists of two cells types: amacrine cells and ganglion cells. The top layer of cells corresponds to amacrine cells and the bottom layer to ganglion cells. Connections from one amacrine cell are shown (black lines). Note that each retinal ganglion cell or amacrine cell receives inputs from many other amacrine cells (not shown; see Experimental Procedures for details). When a sufficiently high fraction of amacrine cells become active, a simulated wave will pass through those amacrine cells (red) and be relayed to a contiguous distribution of ganglion cells (blue). Spontaneously active amacrine cells not correlated with the wave are shown in gray.

(B) Waves generated by computer simulation of the two-layer readout model are influenced by the past activity of amacrine cells. The top frame of each pair corresponds to all of the activity in the network that occured during the time evolution of a simulated wave (as indicated by arrows from the time bar), i.e., activity in the ganglion cell layer (blue areas), in the amacrine cells that participate in that wave (red dots), and in amacrine cells that are active but do not participate in the wave (gray dots). The bottom frame contains pseudocolor plots which indicate the number of amacrine cells available to participate in a wave (i.e., not refractory) in the time step immediately preceding the initiation of a wave. The color bar corresponds to the fraction of nonrefractory cells (0%–50%). For more information, consult Segment 2 of the video of simulated waves accompanying this paper at www.neuron.org.

zones of potential wave activity. In contrast, wave boundaries are restricted by blue regions, since waves cannot propagate through areas containing a high fraction of refractory amacrine cells. In the model, regions that previously supported a wave become refractory (blue) as the cells that participated in the wave enter their refractory period in subsequent frames. Furthermore, regions that did not support a wave but had a substantial level of amacrine cell activity can also become blue.

This analysis also suggests a possible origin of the refractory period measured in the ganglion cell layer. Recall that in our model, the ganglion cells do not have an intrinsic refractory period. Rather, the intrinsic refractory period of the amacrine cells, combined with a ganglion cell threshold for firing, confers an effective refractory period to the visualized tissue. In the model, the refractory period measured in the ganglion cell layer is therefore a collective property of the amacrine–ganglion network.

The Two-Layer Model Is Consistent with the Periodicity, Size, and Velocity of Retinal Waves

In this section, we quantitatively compare observed and simulated retinal waves using two statistical measures to characterize their spatiotemporal properties. First, we used the time interval between successive waves traversing a given retinal location to study the temporal regularity of the activity. Experimentally, the distribution of these interwave intervals is broad (Figure 5A), showing that while there is a characteristic time interval between waves, they are not strictly periodic. The lower bound of the interwave interval distribution is determined by the minimum refractory period, but the interwave interval distribution peaks near 2 min, which is two to three times the measured refractory period. The ratio of the interwave interval to the refractory period is a critical parameter and severely restricts the possible circuitry responsible for wave generation (see discussion of the one-layer model below).

The second statistical property we characterized was the domain size distribution. Note that a distinctive property of the waves that must be taken into account by any model is the compact (i.e., not sparse) nature of the domains. We plotted the domain size distributions by measuring the area of retina covered by each wave (Figure 1). Domain size histograms for five retinas are shown in Figure 5B. Like the interwave interval distributions, the area distributions are extremely broad, showing that a given retina supports a wide range of domain

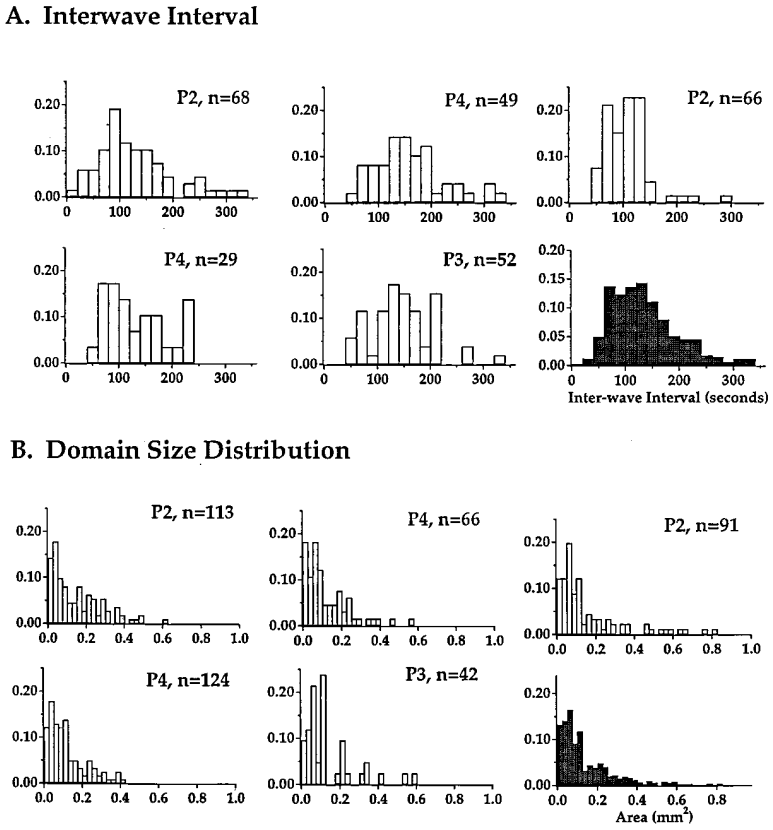

Figure 5. Summary of Spatiotemporal Properties

(A) Interwave interval distributions observed for five retinas. The interwave interval distribution was defined as the time between waves passing through a single point on the retina. Each distribution includes the interwave intervals measured at nine equally spaced points within the field of view. Bin size is 20 s. Shaded plots show the cumulative distribution for all five retinas.

(B) Distribution of domain sizes for the same five retinas as in (A). Bin size is 0.025 mm^2. Note that all waves that appear within the recording area are included in the distribution, including waves whose boundaries stretch outside the field of view. All distributions are normalized to 1.

sizes. Note that some domains are cut off by the edges of the field of view (1.7 mm^2), which slightly skews the distributions toward smaller areas. The smallest domains measured are 0.025 mm^2 (corresponding to a disk 180 μm in diameter); the largest domains measured are 0.8 mm^2. The distribution of domain sizes remains relatively flat for domains measuring up to 0.075 mm^2, the equivalent of a disk 300 μm in diameter, or $\sim$200 cells in the ganglion cell layer (see Experimental Procedures).

Quantitative measures of simulated wave parameters for the two-layer readout model agree well with the experimental results. For example, interwave interval measurements of waves generated by a simulation of the two-layer readout model have a distribution that peaks near twice the refractory period (Figure 6A, middle), in agreement with experiments (Figure 6A, top). The interwave intervals are measured in units of the refractory period as measured in the ganglion cell layer. Note that the peak of the interwave interval distribution of the simulated waves from the two-layer readout model is determined by the amacrine cell refractory period.

There is also good agreement between the domain size distributions of the experimentally-observed and simulated two-layer model waves. In both cases, the distribution remains relatively flat for domain sizes up to $\sim$0.075 mm^2 (Figure 6B, top and middle). The location of the peak in the two-layer model's simulated distribution is roughly set by the number of amacrine cells that are excited by a single amacrine cell (see Experimental Procedures).

To test the predictive ability of the model, we compared how lowering the amacrine cell threshold affects the average wavefront propagation of both simulated and measured waves. (Lowering the ganglion cell threshold has no effect on wavefront velocity, since the ganglion cell layer is only a passive readout.) Propagation velocities for both measured and simulated waves were computed by defining the wave boundaries at discrete time intervals and measuring the distance traveled along a direction nearly perpendicular to the wavefront (Figure 7A, left). The time evolution of an imaged retinal wave (at 500 ms intervals) and simulated wave are shown in Figure 7A (left). The wavefront velocity (the slope of the distance versus time curves) is not constant but instead waves speed up and slow down. On average, the measured waves propagate with a velocity of 177 $\pm$ 67 μm/s (n = 27 waves, 3 retinas), in agreement with earlier recordings using a multielectrode array (Wong et al., 1993). Occasionally, waves accelerate to local wavefront velocities of greater than 500 μm/s, as evidenced by the staircased, rather than smooth, structure of the curves in Figure 7A. This variations in local wavefront velocity is not a property of specific retinal locations, since subsequent waves passing through a given location can travel at widely different speeds (data not shown). The average wavefront velocity for simulated waves was 238 $\pm$ 43 μm/s (15 simulated waves; see Experimental Procedures for a description of how the magnitude of the velocities was computed), which is comparable to the velocities measured experimentally. The model also predicts that fluctuations in wavefront velocity can be attributed directly to the fraction of amacrine cells that are refractory when a wave propagates through a given region. A wavefront will propagate more

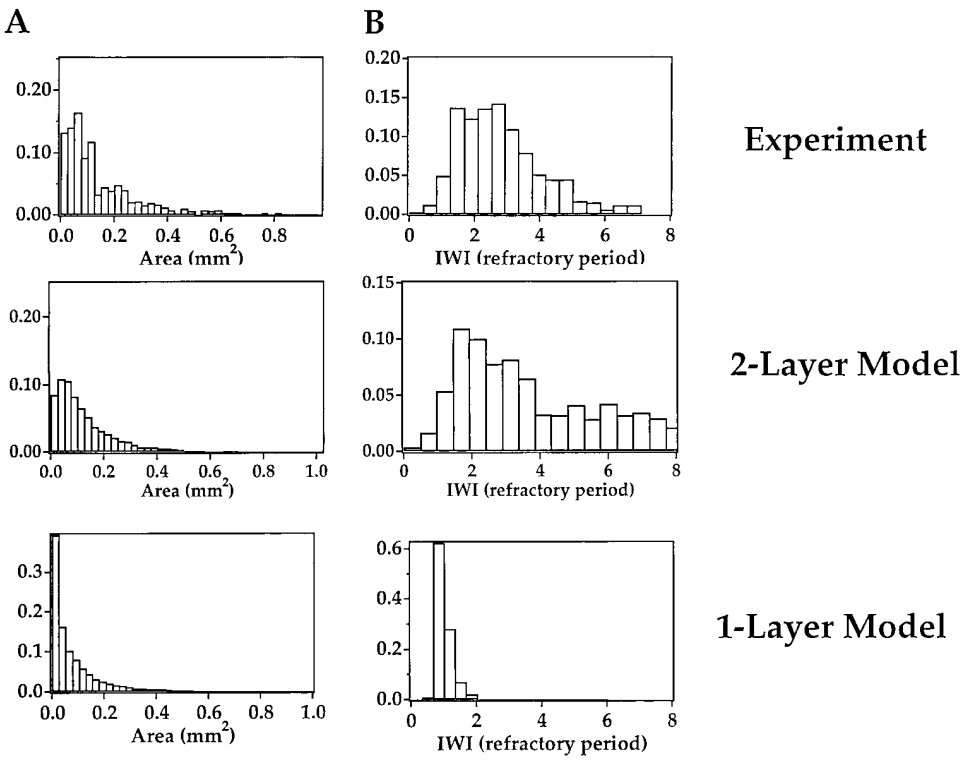

Figure 6. Area and Interwave Interval Distributions Compared with Models

A summary of experimental results for 5 retinas (see Figure 5). (A) shows domain size distributions, and (B) shows interwave interval distributions for waves generated by simulations of the two-layer (middle) and one-layer (bottom) models. Spatial dimensions for domain size distributions were determined by allowing 250 μm^2 for each cell (see Experimental Procedures: Model). Interwave interval distributions for simulated waves were measured at six equally spaced points within the model retina. Cumulative results for the interwave interval are plotted in units of the ganglion cell layer refractory period, which corresponds to the minimum interwave interval recorded (see text). Results from 4876 simulated waves were included in the distributions. All distributions are expressed as a fraction of the total number of waves.

quickly through an area with a high density of nonrefractory amacrine cells (Figure 4B, bottom frames, red regions). Fluctuations in wavefront velocity can be exaggerated by increasing the amount of variability of excitatory input a cell receives. For example, increasing the dendritic spread of amacrine cells would allow for more variation in the number of refractory cells in a given region (data not shown). In the model, as in experiments, subsequent waves passing through a given location travel at different speeds.

Simulated waves showed a 25% increase in average wavefront velocity for a 17% decrease in threshold (Figure 7B, right). To lower the threshold experimentally, we increased the concentration of potassium in the bath from 2.5 mM to 5 mM. This manipulation depolarizes ganglion cells from a resting potential of −53 mV to approximately −45 mV (n = 3 cells, data not shown). As predicted by the model, we found a marked increase in the average wavefront velocities of waves of ~60% (Figure 7B, left histograms). Furthermore, the mean domain size increased, consistent with the simulation (data not shown).

In summary, the two-layer readout model makes several predictions. First, the waves we record experimentally from the ganglion cells using fluorescence imaging are filtered images of the activity in the amacrine cell layer, which is responsible for the initiation and propagation of the waves. Second, the model makes specific predictions concerning the physiological properties of amacrine cell activity—namely, that amacrine cells have spontaneous activity that is not necessarily correlated with waves. The model further implies that amacrine cells or amacrine-to-ganglion cell synapses have a long refractory period that sets the measured periodicity of wave activity. Finally, the initiation and propagation of waves (as measured in the ganglion cell layer) are determined by the past history of excitation in the amacrine cell layer.

Wave Properties Are Not Consistent with a One-Layer Model

Are two independent cell types required to reproduce the statistical properties of waves? To test this, we introduced a specific class of one-layer models of the retina. This naive model consists of a homogeneous population of units with two properties: a finite probability of spontaneous activation, and a refractory period. Wave propagation is mediated through near-neighbor coupling, such that the activity of one unit leads to additional activity of nonrefractory neighbors. Note that a computational unit may be composed of more than one cell type. For instance, if a set of ganglion cells fired every

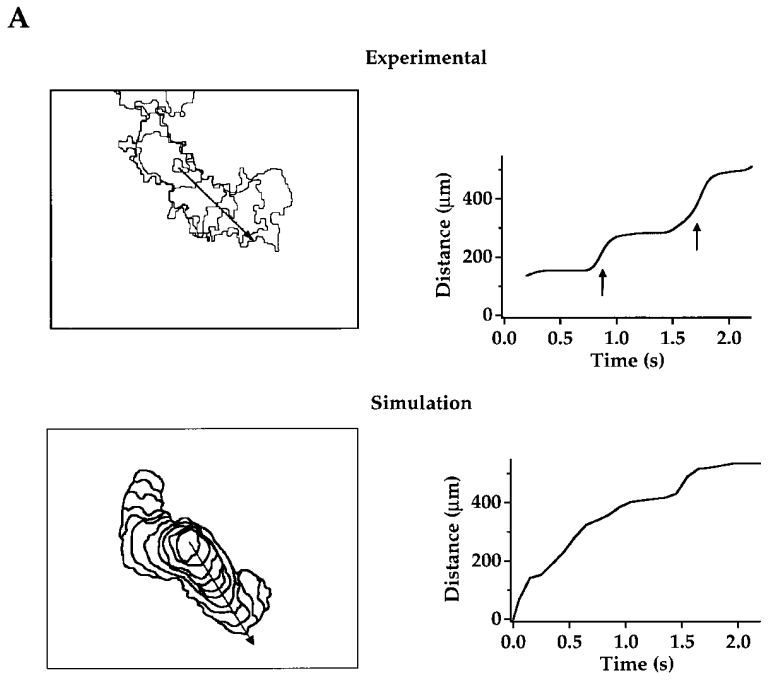

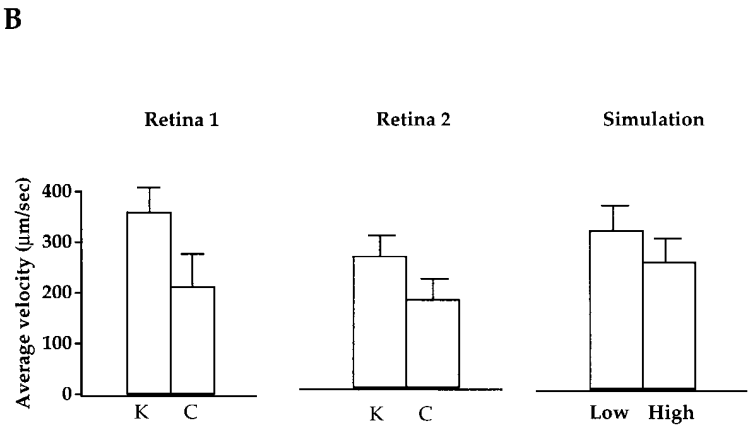

Figure 7. Wavefront Propagation Velocity

(A) Calculation of wavefront velocities. On the left are wave boundaries of an imaged wave shown at 500 ms intervals (top) and a wave generated by computer simulation of the two-layer readout model at 200 ms intervals (bottom). On the right are distance versus time plots. Distances were computed along a straight vector oriented roughly perpendicular to the wavefront (see Experimental Procedures). The curves were smoothed with a binomial filter. Arrows in the top plot show onsets of increased wavefront velocity. The field of view is 1 mm × 1 mm.

(B) Lowering spike threshold increases both experimental and simulated wave velocity. The first two histogram plots (left and middle) compare average velocities computed for waves recorded in normal (C, 2.5 mM) and high (K, 5 mM) concentrations of potassium (two retinas; 10 waves each). The histogram distribution of the average velocity of the simulated waves (15 waves, right) under two conditions are compared for a normal and decreased amacrine cell threshold.

time an amacrine cell fired, and this unit was repeated to make up the entire retinal network, such a network would also be classified as a one-layer model. The essential property is that each unit is characterized by a single measure of activity. By contrast, in the two-layer model, a local patch of amacrine and ganglion cells cannot be lumped together since one may be active without the other.

In this class of one-layer model, the refractory period is the sole determinant of wave boundaries. A simple argument shows, however, that this requirement would only allow for interwave intervals that are roughly equal to the refractory period (Figure 6B, bottom): if the interwave interval were much longer than the refractory period, then every wave would propagate across the entire retina, since then the entire retina would be reset by the time the new wave arrives. As was illustrated in Figure 1, however, waves are limited in their spatial extent to domains of defined sizes. Since the interwave interval distribution peaks at twice the refractory period (Figure 6B, bottom), something other than the refractory period must determine wave boundaries.

As mentioned earlier, not all wave boundaries are delimited by refractory regions (Figure 1). Within a one-layer model, the only other possible means of limiting the spatial extent of a wave would be failure of the coupling mechanism: when a given unit fires, its neighbors may not fire, interrupting the propagation of the wave. If this were the case, smaller waves would be more frequent than larger ones, and the distribution of domain sizes would be a monotonically decreasing function, peaked at the smallest domains (Figure 6A, bottom).

Results above indicate that a simple one-layer model— consisting of a single computational unit that is spontaneously active, with a refractory period, and whose activity is transferred to its near neighbors—is inconsistent with the measured qualitative and quantitative properties of retinal waves. We conclude that the spatiotemporal properties of retinal waves cannot be

described by such a one-layer model. Of course, we cannot rule out more complicated one-layer models. In contrast, our two-layer model involves at least two computational units, where one unit may be active without the other.

Discussion

We have presented a physiologically realistic model that shows that a simple network involving only two cell types can reproduce robustly the spatiotemporal patterns of retinal waves. We used fluorescence imaging to reveal that the spatial location of wave initation sites, and the boundaries that limit wave propagation, are not set by fixed structures but arise from dynamic properties of the immature retinal network. The predictions of the model, in combination with the experimental observations, allow us to describe how the physiological properties of individual neurons can cooperatively generate intrinsic large-scale patterns of correlated activity. In this section, we first discuss the validity of the assumptions made for the model in terms of known anatomical and physiological properties of the immature retina. We then present arguments that describe how retinal waves might be generated by the developing retinal circuitry based on experimental observations, the predictions of the two-layer readout model, and comparisons to other neuronal structures that display similar behavior. Finally, we make predictions about how these patterns of activity might influence the patterning of connections in the retina itself. A more detailed description of the quantitative features of the model will be presented elsewhere.

Validity of Model Assumptions and Predictions

A primary prediction of the two-layer readout model is that a class of cells with properties distinct from those of the ganglion cells is responsible for the initiation, propagation, and termination of waves. Retinal waves are known to involve a network containing at least two cell types, amacrine and ganglion cells (Wong et al., 1995; Feller et al., 1996). Retinal ganglion cells have both cholinergic and GABAergic postsynaptic currents during waves; however, only the cholinergic input is required for wave propagation, at least at the earliest ages studied here (Feller et al., 1996; but see also Shields et al., 1996, Invest. Ophthalmol. Vis. Sci., abstract, and discussion below). We therefore propose that the readout activity is generated by cholinergic amacrine cells, and for simplicity we assume that they are the only type of amacrine cell in our model network.

Amacrine and Ganglion Cell Physiology

In the model, we make many assumptions about the physiological properties of cholinergic amacrine cells (reviewed by Masland and Tauchi, 1986; Vaney, 1990). First, we assume that amacrine cells are spontaneously active, but that their activity does not always result in a wave in the ganglion cell layer. Spontaneous activity is not likely to be mediated by glutamatergic inputs from bipolar cells, as it is in adult cholinergic amacrine cells (Taylor and Wassle, 1995; Peters and Masland, 1996), since blockade of glutamatergic transmission does not block waves (Wong et al., 1995). Amacrine-to-amacrine synapses may be present, though, raising the possibility that the spontaneous activity of cholinergic amacrine cells could be mediated by other amacrine cells or generated intrinsically in the cholinergic amacrine cells themselves. It will be of great value to make physiological recordings from cholinergic amacrine cells in intact immature retinas (Zhou and Fain, 1996; Zhou, 1997, Invest. Ophthalmol. Vis. Sci., abstract).

In the model, a ganglion cell receives inputs only from amacrine cells, and neither has the ability to depolarize spontaneously nor has a refractory period. We assume that the coupling that is known to exist between ganglion cells (Mastronarde, 1989; Meister et al., 1991; Penn et al., 1994) is not involved in wave generation, implying that the ganglion cell layer serves as a passive filter of the amacrine cell layer activity. We also assume that a ganglion cell participates in a wave only when its excitation level exceeds a threshold. This assumption is consistent with the experimental observation that changes in fluorescence associated with increases in $[Ca^{2+}]_i$ imaged at low magnification are simultaneous with robust bursts of action potentials (Feller et al., 1996) and that blocking action potentials with tetrodotoxin also blocks the waves (Meister et al., 1991; Wong et al., 1995).

Refractory Period

A central prediction of our model is that the spatial extent of waves is not defined by predetermined structures within the retina, but is instead determined by fluctuating levels of excitability in the amacrine cell layer. These dynamic boundaries are in significant contrast to repeating domain boundaries defined by the spontaneous propagating activity observed in developing neocortex (Yuste et al., 1992) as well as the spindle waves in the thalamus, which propagate across the entire structure (Kim et al., 1995).

The two-layer readout model predicts that the refractory period measured in the ganglion cell layer arises from a combination of a longer refractory period in amacrine cells plus a ganglion cell threshold. In the model, after they are depolarized past threshold, amacrine cells enter this refractory period, during which time they cannot be spontaneously depolarized or excited by their neighbors. The source of this refractory period is not yet understood, but could be due to large after-hyperpolarizing currents in cholinergic amacrines (Taylor and Wassle, 1995), similar to those thought to underlie the refractory periods seen in thalamic spindle waves (Kim et al., 1995) and the waves that propagate across the procerebral lobe, an olfactory organ, of Limax maximus (Delaney et al., 1994; Kleinfeld et al., 1994). Another possibility is that α-bungarotoxin-insensitive neuronal nicotinic receptors on either amacrine or ganglion cells become desensitized following participation in a wave (McGehee and Role, 1995; Feller et al., 1996). An intriguing possibility is that this refractory period is associated with a cellular process such as the refilling of internal calcium pools (Yao et al., 1995), which is known to set the refractory period for calcium waves seen in Xenopus laevis oocytes, or perhaps with the refilling of a readily releasable pool of synaptic vesicles, as has been studied in hippocampal neurons (Stevens and Tsujimoto, 1995).

Wave Initiation and Propagation

We have shown that the initiation sites of waves are distributed uniformly across the retina (Figure 3). This observation is reflected in the model, where all amacrine cells have the same rate of spontaneous depolarization; wave initiation is due solely to spontaneous activity in the amacrine cell layer, when a sufficient number of nearby amacrine cells become coactive (Figure 4B). This situation contrasts with that known to occur in other neural structures exhibiting activity correlated across many cells, where the initiation region contains a high density of pacemaker or trigger cells (Johnson et al., 1994; Yuste et al., 1995; Marder and Calabrese, 1996) or where there is some variation in local circuitry that makes one area of tissue more excitable (Destexhe et al., 1994; Kim et al., 1995; Charles et al., 1996). The model assumes that the horizontal spread of the excitation occurs through amacrine-to-amacrine cell connections. In the simplest scenario for wave propagation through the amacrine cell layer, cholinergic amacrine cells would respond to acetylcholine (Millar and Morgan, 1987; Mariani and Herch, 1988; Famiglietti, 1991; but see also Baldridge, 1996).

Amacrine cells may also communicate through a GABAergic circuit, since cholinergic amacrine cells contain (Vaney and Young, 1988; Brecha et al., 1988) and respond to GABA (Zhou and Fain, 1995) and may corelease GABA with acetylcholine (O'Malley et al., 1992). Though at the earliest ages studied (P0–P5) we have found that the $GABA_A$ antagonist SR95531 has no effect on wave generation (Feller et al., 1996), recent findings in slightly older animals ($>$P12) suggest that GABA blockers can influence the temporal patterns of retinal waves (Shields et al., 1996, Invest. Ophthalmol, Vis. Sci., abstract), which supports the hypothesis that cholinergic amacrine cells might be modulated by GABA. A third possibility is that excitation within the amacrine cell layer is mediated through secretion of neuromodulators, like adenosine or dopamine (Blazynski et al., 1992; Hare and Owen, 1995). We emphasize that our model presents the simplest scenario—namely, that cholinergic amacrine cells are involved in wave initiation. The model is entirely consistent with the idea that excitation is relayed through other amacrine cell types as well as the cholinergic cells, or even with the idea that one amacrine cell type is spontaneously active, while the cholinergic amacrine cells are simply a necessary component of the horizontal circuitry needed for relay of excitation.

Uniqueness and Robustness of the Two-Layer Model

We have argued that the two-layer readout model is the simplest model that is capable of generating the spatiotemporal properties of real waves. Of course, this does not permit us to rule out models based on more complicated computational units. Nevertheless, any successful model must be able to account for (a) the source of spontaneous activity, (b) the propagation of this activity in a compact, finite wave, and (c) the discrepancy between the time interval between waves and the refractory period. Our model, however, accounts for these properties by making the following assumptions, which are consistent with the known properties of the immature retina. First, we include spontaneous activity in the amacrine cell layer, since some source of initiation must be present in the network, and the ganglion cells are known not to be spontaneously active. Second, activity in the amacrine cell layer is subject to a refractory period, but can also propagate from cell to cell over the known dendritic spread of these cells. This accounts for the minimal size of the waves and the minimal interval between waves at a given location. Third, the ganglion cell layer provides a passive filter of amacrine cell activity. Filtering the amacrine cell activity is necessary to simultaneously account for the compactness of the waves and the discrepancy between measured interwave intervals and the refractory period, as discussed in the Results.

Though the exact nature of the cellular mechanisms underlying the model are not known, the model does not require exquisitely fine tuning to account for observed wave properties. As discussed in the Experimental Procedures, for a given set of fixed (i.e., anatomical) parameters, there is some range of free parameters (thresholds and spontaneous activity rate) that generate waves that qualitatively and quantitatively resemble the observed waves. This point is significant on two levels. First, it shows that the reproduction of the experimental properties is a general feature of the architecture of the two-layer readout model and not a unique property of the parameters we have used. There is also a second and more profound implication: if a simple model neural circuit can generate wave behavior without requiring fine adjustment of parameters, then we may expect that wave behavior in the real circuit is not sensitive to the precise biophysical properties of immature neuronal networks. The validity of the model is strengthened by experiments that show that lowering the amacrine cell threshold leads to consistent changes in wave properties in both simulated and experimentally measured waves, namely an increase in average wave velocity (Figure 7).

Implication of Wave Dynamics for Visual System Development

Retinal waves occur at an age when the wiring of many structures within the visual system is immature and highly plastic (Bodnarenko and Chalupa, 1993; Sernagor and Grzywacz, 1996; Wong and Oakley, 1996). At the same time, retinal ganglion cell axon terminals in the lateral geniculate nucleus are first segregating into eye-specific layers (Shatz, 1996), and then further segregating into ON–OFF layers (Garraghty and Sur, 1993). Waves might also be important for development of circuitry within the retina, since the period of wave activity (Wong et al., 1993) coincides with a period of extensive retinal development (Ramoa et al., 1988; Wingate, 1996). It has been well established that the segregation of ganglion cell dendrites into ON–OFF sublaminae in the inner plexiform layer is activity dependent (Bodnarenko and Chalupa, 1993). Furthermore, recent experiments in the turtle retina show that blocking wave activity prevents the dark rearing-induced expansion of ganglion cell receptive fields (Sernagor and Grzywacz, 1996), implying

that correlated activity is involved in establishment of local circuitry. An interesting prediction made by the two-layer readout model is that amacrine cell and ganglion cell activities are correlated to differing extents. There are three types of correlations possible between a pair of amacrine and ganglion cells. During a wave in the ganglion cell layer, only a fraction of the amacrine cells that are synaptically connected are involved, implying that either both cells are simultaneously above threshold (Figure 4B, top row, red and blue cells) or that the ganglion cell is depolarized above threshold while the amacrine cell is inactive. In addition, amacrine cells can depolarize spontaneously, independent of a wave in the ganglion cell layer (Figure 4B, top row, gray cells), so that an amacrine cell can be active without postsynaptic ganglion cells being depolarized above threshold. These various scenarios predicted by our model allow for a wide range of activity-dependent mechanisms that could be involved in refinement of local circuitry within the retina.

We have shown that the precise spatiotemporal properties of retinal waves can be generated robustly by a simple neuronal circuit. The general principle that the activity of the cells within the circuit is influenced by their past history of activity, combined with spontaneous activity of individual cells, is sufficient to create rhythmic, correlated, spontaneous activity. This can be achieved without fine-tuning the details of the connectivity or biophysical properties of individual cells. This approach of using crude, early-forming circuits to generate precise patterns of activity may be a general strategy used by a variety of circuits throughout the nervous system to refine imprecise wiring within the circuits themselves and within their targets.

Table 1. Model Parameters Used for Simulated Waves Analyzed in Figure 6

Fixed Parameters	
Timestep: $\Delta t = 100$ ms	
Firing time: $T_F = 1$ s	
Integration time of amacrine cell: $\tau_A = 0.1$ s	
Amacrine cell input radius*: $R_A = 120$ μm in diameter	
Mean refractory period distribution: $T_R = 120$ s	
Variance of refractory period distribution: $\Delta T_R = 38$ s	
Integration time of ganglion cell: $\tau_G = 0.1$ s	
Ganglion cell input radius*: $R_G = 120$ μm in diameter	
Free Parameters	
Probability of spontaneous firing rate: $p = 0.035$ s^{-1}	(0.03–0.045)
Amacrine cell threshold: $\theta_A = 6$ units	(5–6)
Ganglion cell threshold: $\theta_G = 10$ units	(7–13)

*Radius over which cell receives input from nearby amacrine cells

The model is completely determined by two sets of parameters, "fixed" and "free". Fixed parameters are determined by the anatomy and physiology of the retinal ganglion cells and cholinergic amacrine cells. Free parameters are chosen to reproduce the spatiotemporal properties of retinal waves. The range of variables listed in parentheses refer to values that lead to waves that are qualitatively and quantitatively similar to those shown in Figure 6. Simultaneous variation of two parameters is not discussed here. See the Experimental Procedures for details and references.

Experimental Procedures

Retina Preparation

Eleven retinas were isolated from newborn (P0–P10) ferrets that had been deeply anesthetized with halothane and then decapitated. All procedures were performed in artifical cerebrospinal fluid (ACSF; 119 mM NaCl, 2.5 mM KCl, 1.3 mM $MgCl_2$, 10.0 mM KH_2PO_2, 2.5 mM $CaCl_2$, 26.2 mM $NaHCO_3$, and 11 mM D-glucose). Solutions were buffered with $NaHCO_3$ and oxygenated with a mixture of 95% O_2 and 5% CO_2. Isolated retinas adhered to filter paper were incubated in fura-2AM as described previously (Feller et al., 1996). The retinas and filter papers were placed in a temperature controlled chamber (31°C–34°C; Medical Systems), mounted on the stage of an inverted microscope (Nikon, Diaphot 200), and continuously perfused.

Wave Definition and Analysis

Waves were acquired using fluorescence imaging methods previously described (Feller et al., 1996) and stored on Hi8 videotape. An initial background frame was subtracted from all subsequent images to create ΔF, or difference images of the retina. Individual videoframes of difference images were acquired at 0.5 s intervals from a computer-controlled video editor (Sony 118) onto a Macintosh computer using NIH Image. All domains were defined using the same computer algorithm, which consisted of a series of filters to remove high frequency noise and enhance contrast. Thresholding of the processed image was done through an iterative selection procedure (Ridler and Calvard, 1978). The individual frames were combined to define the area covered by a wave. The wave initiation point was determined by the centroid of the first processed and thresholded frame in which a wave appeared. The velocity of the wavefront was computed by acquiring successive frames from the videotape at 33 ms intervals, processed as described above. The direction along which the velocity was computed was determined by the line that represented the longest distance traveled by the wave and that was nearly perpendicular to the wavefront at all intersection points.

Model

We modeled the wave-generating circuitry of the developing mammalian retina by a pair of coupled, two-dimensional networks that represent the retinal ganglion cell and cholinergic amacrine cell layers, respectively. The simulation was implemented using Borland C++ on a Pentium PC and Cray C++ on a T3E supercomputer. The statistical properties of the simulations were analyzed in an analogous manner to the experimental data. The parameters listed in Table 1 provide a complete specification of the model.

Spatial Organization of Networks

The amacrine cell layer was modeled as a close-packed triangular lattice of cells (see Figure 4A) with a lattice spacing of 34 μm, based on immunohistological staining for choline acetyltransferase in developing ferret retinas of comparable ages (Feller et al., 1996). For simplicity, the ganglion cell layer was also modeled as a triangular lattice with one-half the lattice spacing of the amacrine cells (17 μm), which is consistent with a cell soma diameter of 12 μm (Ramoa et al., 1988), with only 50% of cells participating in waves (Wong et al., 1995). To match the field of view used in the imaging experiments, the model ganglion cell layer was 96×70 cells, representing a patch of retina 1.4 mm $\times$ 1.2 mm.

Results from the simulation show that the area over which a given model amacrine cell receives excitatory inputs roughly sets the peak of the domain size distribution generated by the simulation (see Results). We therefore assume that an amacrine cell receives inputs from the surrounding 0.05 mm^2, corresponding to the peak in the experimental domain size distribution (see Figure 4B); a given amacrine cell provides inputs to cells at a distance of up to 120 μm away, which we define as the input radius, R_A. This value is consistent with the measured dendritic spread of cholinergic amacrine cells in the developing retinas of rabbit (Wong and Collin, 1989) and cat (Dann, 1989; Mitrofanis et al., 1989). In the model, each amacrine cell is synaptically connected with equal strength to other amacrine cells within its input radius, which is roughly seven ganglion cells or three to four amacrine cells. Ganglion cells integrate inputs from the amacrine cell processes that lie within their input radius, R_G, which we also set to be $\sim$120 μm, consistent with measurements in the embryonic cat retina (Ramoa et al., 1988). The connections

from amacrine cells to ganglion cells are purely feed forward, i.e., the state of the amacrine cells affects the state of the ganglion cells, but not vice versa.

Temporal Behavior of Cells

The elementary time step of the model is 100 ms. Details of behavior on shorter time scales are not described by the model. Both amacrine cells and retinal ganglion cells are modeled as leaky integrate-and-fire neurons. A given cell is characterized by an excitation level, X, which is analogous to the amount of membrane depolarization away from the cell's resting potential. Inputs from other neurons raise the excitation level with an integration time, τ, set to 100 ms for both amacrine and ganglion cells (Velte and Miller, 1995). When the excitation level exceeds the neuron's threshold, θ, the cell is said to fire. For ganglion cells, θ_G corresponds to spike threshold; for amacrine cells, θ_A is the threshold for synaptic transmission.

Under the feed-forward assumption of our model, ganglion cell firing does not affect other cells in the network, but simply allows them to be visualized in the simulation. On the other hand, firing amacrine cells provide inputs to both amacrine cells and ganglion cells within their dendritic spreads. Their firing time, T_F, is set to be 1 s. While firing, they raise the excitation levels of their neighbors by one unit. The time evolution of the excitation level of a given amacrine and ganglion cell over time Δt is given by:

$$X^A_{i,new} = X^A_{i,old} e^{-\Delta t/\tau_A} + N^A_i$$

$$X^G_{j,new} = X^G_{j,old} e^{-\Delta t/\tau_G} + N^A_j$$

where N^A_i is the number of firing amacrine cells within cell i's dendritic arbor. After firing, the neuron's excitation level is reset to zero. Amacrine cells (but not ganglion cells) are then held at zero for the duration of their refractory period. Before the simulation begins, each amacrine cell is assigned a refractory period, such that the distribution of refractory periods is Gaussian with a mean T_R and a standard deviation ΔT_R. The mean refractory period is set to the experimental peak in the interwave interval distribution, and the standard deviation is set to be 25%.

Finally, the model must contain some intrinsic excitability; otherwise it will eventually become completely inactive (all $X_i = 0$) due to the built-in decay of excitation levels. Since waves initiate randomly across the retina, we infer that there are no special pacemaker cells or regions in the developing retina (Figure 3). To introduce excitability into the model in the simplest possible manner, each amacrine cell is given a probability p of firing spontaneously in a given time step, regardless of its current excitation level. We set p to reproduce the experimentally measured initiation rate of 3 waves/min/mm^2 (data not shown). Except for this feature, our model is otherwise completely deterministic.

Free Parameter Values

There are three free parameters that are poorly constrained by previous experiments: the rate of spontaneous activity of amacrine cells, the threshold of amacrine cells, and the threshold of ganglion cells. These variables are given plausible values that yield excellent qualitative and quantitative agreement between the spatiotemporal dynamics of experimentally measured retinal waves and those waves generated by computer simulation of the model. Within this defined parameter space, the behavior of the model is highly dependent on the physiological properties of amacrine cells, namely the spontaneous rate of firing p and the threshold θ_A. Small changes in the properties of ganglion cells, however, have little effect on the properties of the simulated waves. Since the ganglion cell layer acts as a readout of the activity in the amacrine cell layer, the only constraint on the ganglion cell threshold is that it must distinguish between wave and nonwave behavior of the amacrine cell layer. The depolarization of a given ganglion cell resulting from uncorrelated amacrine cell activity (Figure 4, top row, gray cells) is much less than the depolarization produced by correlated amacrine cell activity in a wave (Figure 4, top row, red cells). This situation does not require fine-tuning of the ganglion cell threshold.

The setting for the amacrine cell threshold θ_A, however, strongly affects the simulation behavior by influencing wave initiation and termination. If θ_A is too high, there will be very few wave initiations, since a high amacrine cell threshold would require a high rate of spontaneous amacrine cell depolarizations to generate sufficient correlated amacrine cell activity to depolarize the ganglion cells above their threshold. If θ_A is too low, waves spread over the entire retina, since excitation traveling into low-threshold regions needs only to recruit a few nonrefractory amacrine cells for propagation. We therefore set the amacrine cell threshold within the range where there are a sufficient number of finite-sized waves. As mentioned in the Results, varying θ_A within this range does affect the domain size distribution and wave velocities (Figure 7B).

The statistical properties of the simulated waves also depend on the value of the spontaneous rate of firing, p. We used a high rate for the simulations ($\sim$0.035 s^{-1}) to guarantee that a nonrefractory amacrine cell will spontaneously depolarize in a time interval ($\sim$1/p, or 30 s) much shorter than its refractory period ($\sim$2 min); this value leads to an initiation rate comparable to that seen experimentally. If p is set much higher, then very few larger waves occur, since high levels of spontaneous activity not correlated with waves will make larger regions of the amacrine cell layer refractory at any given time, thereby preventing extended propagation of the wave (Figure 4B).

Velocity Measurements of Simulated Waves

Waves in the simulation were recorded and stored as a list of each participating ganglion cell and the time that it became active. The initiation point was determined by the average position of the ganglion cells active in the first time step. The participating ganglion cells were then sorted into 16 groups according to their relative direction from this initiation point. From each direction group, the farthest active cell from the initiation point in each time step was used to define the distance the wave traveled in that given direction as a function of time, and the resulting curve was smoothed using a box filter corresponding to five timesteps. The mean velocity was then determined by the slope of the best linear fit to this distance versus time, not including the time step corresponding to the initiation time (the fit did not have to go through the origin). Mean wavefront velocity for a given set of parameters was calculated using 15 individually acquired waves from the simulation running with those parameters.

Acknowledgments

The authors wish to thank David Stellwagen, Kevin Li, and Raymond Yakura for assistance in image processing. This work was supported by National Science Foundation grant IBN9319539 and National Institutes of Health grant MH 48108 to C. J. S., a Miller Institute Postdoctoral Fellowship to M. B. F., and National Science Foundation grant DMR-91–57414 to D. S. R. D. S. R. and D. A. B. were supported by Lawrence Berkeley National Laboratory grant LDRD-3669–57 and acknowledge the use of the Cray T3E at the National Energy Research Scientific Computing Center. C. J. S. is an Investigator of the Howard Hughes Medical Institute.

Received May 13, 1997; revised July 23, 1997.

References

Baldridge, W.H. (1996). Optical recordings of the effects of cholinergic ligands on neurons in the ganglion cell layer of mammalian retina. J. Neurosci. *16*, 5060–5072.

Blazynski, C., Woods, C., and Mathews, G.C. (1992). Evidence for the action of endogenous adenosine in the rabbit retina: modulation of the light-evoked release of acetylcholine. J. Neurochem. *58*, 761–767.

Bodnarenko, S.R., and Chalupa, L.M. (1993). Stratification of ON and OFF ganglion cell dendrites depends on glutamate-mediated afferent activity in the developing retina. Nature *364*, 144–146.

Brecha, N., Johnson, D., Peichl, L., and Wassle, H. (1988). Cholinergic amacrine cells of the rabbit retina contain glutamate decarboxylase and gamma-aminobutyrate immunoreactivity. Proc. Natl. Acad. Sci. USA *85*, 6187–6191.

Burgi, P.Y., and Grzywacz, N.M. (1994). Model for the pharmacological basis of spontaneous synchronous activity in developing retinas. J. Neurosci. *14*, 7426–7439.

Charles, A.C., Kodali, S.K., and Tyndale, R.F. (1996). Intercellular calcium waves in neurons. Mol. Cell Neurosci. *7*, 337–353.

Cline, H.T. (1991). Activity-dependent plasticity in the visual systems of frogs and fish. Trends Neurosci. *14*, 104–111.

Dann, J.F. (1989). Cholinergic amacrine cells in the developing cat retina. J. Comp. Neurol. *289*, 143–155.

Delaney, K.R., Gelperin, A., Fee, M.S., Flores, J.A., Gervais, R., Tank, D.W., and Kleinfeld, D. (1994). Waves and stimulus-modulated dynamics in an oscillating olfactory network. Proc. Natl. Acad. Sci. USA *91*, 669–673.

Destexhe, A., Contreras, D., Sejnowski, T.J., and Steriade, M. (1994). A model of spindle rhythmicity in the isolated thalamic reticular nucleus. J. Neurophysiol. *72*, 802–818.

Famiglietti, E.V. (1991). Synaptic organization of starburst amacrine cells in rabbit retina: analysis of serial thin sections by electron microscopy and graphic reconstruction. J. Comp. Neurol. *309*, 40–70.

Feller, M.B., Wellis, D.P., Stellwagen, D., Werblin, F.S., and Shatz, C.J. (1996). Requirement for cholinergic synaptic transmission in the propagation of spontaneous retinal waves. Science *272*, 1182–1187.

Garraghty, P.E., and Sur, M. (1993). Competitive interactions influencing the development of retinal axonal arbors in cat lateral geniculate nucleus. Physiol. Rev. *73*, 529–545.

Goodman, C.S., and Shatz, C.J. (1993). Developmental mechanisms that generate precise patterns of neuronal connectivity. Cell *72*, 77–98.

Hamassaki-Britto, D.E., Gardino, P.F., Hokoc, J.N., Keyser, K.T., Karten, H.J., Lindstrom, J.M., and Britto, L.R. (1994). Differential development of α-bungarotoxin-sensitive and α-bungarotoxin-insensitive nicotinic acetylcholine receptors in the chick retina. J. Comp. Neurol. *347*, 161–170.

Hare, W.A., and Owen, W.G. (1995). Similar effects of carbachol and dopamine on neurons in the distal retina of the tiger salamander. Vis. Neurosci. *12*, 443–455.

Hutchins, J.B., Bernanke, J.M., and Jefferson, V.E. (1995). Acetylcholinesterase in the developing ferret retina. Exp. Eye Res. *60*, 113–125.

Johnson, S.M., Smith, J.C., Funk, G.D., and Feldman, J.L. (1994). Pacemaker behavior of respiratory neurons in medullary slices from neonatal rat. J. Neurophysiol. *72*, 2598–2608.

Katz, L.C., and Shatz, C.J. (1996). Synaptic activity and the construction of cortical circuits. Science *274*, 1133–1138.

Kim, U., Bal, T., and McCormick, D.A. (1995). Spindle waves are propagating synchronized oscillations in the ferret LGNd in vitro. J. Neurophysiol. *74*, 1301–1323.

Kleinfeld, D., Delaney, K.R., Fee, M.S., Flores, J.A., Tank, D.W., and Gelperin, A. (1994). Dynamics of propagating waves in the olfactory network of a terrestrial mollusk: an electrical and optical study. J. Neurophysiol. *72*, 1402–1419.

Maffei, L., and Galli-Resta, L. (1990). Correlation in the discharges of neighboring rat retinal ganglion cells during prenatal life. Proc. Natl. Acad. Sci. USA *87*, 2861–2864.

Marder, E., and Calabrese, R.L. (1996). Principles of rhythmic motor pattern generation. Physiol. Rev. *76*, 687–717.

Mariani, A.P., and Herch, L.B. (1988). Synaptic organization of cholinergic amacrine cells in the rhesus monkey retina. J. Comp. Neurol. *267*, 269–280.

Masland, R.H. (1977). Maturation of function in the developing rabbit retina. J. Comp. Neurol. *175*, 275–286.

Masland, R.H., and Tauchi, M. (1986). The cholinergic amacrine cells. Trends Neurosci. *9*, 218–223.

Maslim, J., and Stone, J. (1986). Synaptogenesis in the retina of the cat. Brain Res. *373*, 35–48.

Mastronarde, D.N. (1989). Correlated firing of retinal ganglion cells. Trends Neurosci. *12*, 75–80.

McGehee, D.S., and Role, L.W. (1995). Physiological diversity of nicotinic acetylcholine receptors expressed by vertebrate neurons. Annu. Rev. Physiol. *57*, 521–546.

Meister, M., Wong, R.O., Baylor, D.A., and Shatz, C.J. (1991). Synchronous bursts of action potentials in ganglion cells of the developing mammalian retina. Science *252*, 939–943.

Millar, T.J., and Morgan, I.G. (1987). Cholinergic amacrine cells in the rabbit retina synapse onto other cholinergic amacrine cells. Neurosci. Lett. *74*, 281–285.

Mitrofanis, J., Maslim, J., and Stone, J. (1989). Ontogeny of catecholaminergic and cholinergic cell distributions in the cat's retina. J. Comp. Neurol. *289*, 228–246.

Mooney, R., Madison, D.V., and Shatz, C.J. (1993). Enhancement of transmission at the developing retinogeniculate synapse. Neuron *10*, 815–825.

Mooney, R., Penn, A.A., Gallego, R., and Shatz, C.J. (1996). Thalamic relay of spontaneous retinal activity prior to vision. Neuron *17*, 863–874.

Nishimura, Y., and Rakic, P. (1987). Synaptogenesis in the primate retina proceeds from the ganglion cells toward the photoreceptors. Neurosci. Res. Suppl. *6*, S253–S268.

O'Malley, D.M., Sandell, J.H., and Masland, R.H. (1992). Co-release of acetylcholine and GABA by the starburst amacrine cells. J. Neurosci. *12*, 1394–1408.

Penn, A.A., Wong, R.O., and Shatz, C.J. (1994). Neuronal coupling in the developing mammalian retina. J. Neurosci. *14*, 3805–3815.

Peters, B.N., and Masland, R.H. (1996). Responses to light of starburst amacrine cells. J. Neurophysiol. *75*, 469–480.

Ramoa, A.S., Campbell, G., and Shatz, C.J. (1988). Dendritic growth and remodeling of cat retinal ganglion cells during fetal and postnatal development. J. Neurosci. *8*, 4239–4261.

Ridler, T.W., and Calvard, C. (1978). Picture thresholding using an iterative selection method. IEEE Trans. Syst. Man Cybernet. *SMC-8*, 630–632.

Sernagor, E., and Grzywacz, N.M. (1996). Influence of spontaneous activity and visual experience on developing retinal receptive fields. Curr. Biol. *6*, 1503–1508.

Shatz, C.J. (1996). Emergence of order in visual system development. Proc. Natl. Acad. Sci. USA *93*, 602–608.

Stevens, C.F., and Tsujimoto, T. (1995). Estimates for the pool size of releasable quanta at a single central synapse and for the time required to refill the pool. Proc. Natl. Acad. Sci. USA *92*, 846–849.

Taylor, W.R., and Wassle, H. (1995). Receptive field properties of starburst cholinergic amacrine cells in the rabbit retina. Eur. J. Neurosci. *7*, 2308–2321.

Vaney, D.I. (1990). The mosaic of amacrine cells in the mammalian retina. Prog. Ret. Res. *9*, 49–100.

Vaney, D.I., and Young, H.M. (1988). GABA-like immunoreactivity in cholinergic amacrine cells of the rabbit retina. Brain Res. *438*, 369–373.

Velte, T.J., and Miller, R.F. (1995). Dendritic integration in ganglion cells of the mudpuppy retina. Vis. Neurosci. *12*, 165–175.

Wingate, R.J. (1996). Retinal ganglion cell dendritic development and its control. Filling the gaps. Mol. Neurobiol. *12*, 133–144.

Wong, R., and Collin, S. (1989). Dendritic maturation of displaced putative cholinergic amacrine cells in the rabbit retina. J. Comp. Neurol. *287*, 164–178.

Wong, R.O., and Oakley, D.M. (1996). Changing patterns of spontaneous bursting activity of on and off retinal ganglion cells during development. Neuron *16*, 1087–1095.

Wong, R.O., Meister, M., and Shatz, C.J. (1993). Transient period of correlated bursting activity during development of the mammalian retina. Neuron *11*, 923–938.

Wong, R.O., Chernjavsky, A., Smith, S.J., and Shatz, C.J. (1995). Early functional neural networks in the developing retina. Nature *374*, 716–718.

Yao, Y., Choi, J., and Parker, I. (1995). Quantal puffs of intracellular Ca^{2+} evoked by inositol trisphosphate in Xenopus oocytes. J. Physiol. (Lond.) *482*, 533–553.

Yuste, R., Peinado, A., and Katz, L.C. (1992). Neuronal domains in developing neocortex. Science *257*, 665–669.

Yuste, R., Nelson, D.A., Rubin, W.W., and Katz, L.C. (1995). Neuronal

domains in developing neocortex: mechanisms of coactivation. Neuron *14*, 7–17.

Zhou, Z.J., and Fain, G.L. (1995). Neurotransmitter receptors of starburst amacrine cells in rabbit retinal slices. J. Neurosci. *15*, 5334–5345.

Zhou, Z.J., and Fain, G.L. (1996). Starburst amacrine cells change from spiking to nonspiking neurons during retinal development. Proc. Natl. Acad. Sci. USA *93*, 8057–8062.